Design, Fabrication, and ML-Based Optimization of a High-Performance Metamaterial Absorber for Emerging Applications

Himanshu Shekhar[1], Gauri Ojha[2], Pranav Gupta[3], Upender Patri[4]
[1,2,3,4]Vellore Institute of Technology, Chennai, Tamil Nadu, India.
Email: upender.p@vit.ac.in

Abstract

This paper presents the design, fabrication, and machine learning (ML)-based optimization of a compact metamaterial absorber (MMA) exhibiting wideband absorption from 7.13–12.22 GHz. The proposed absorber is polarization insensitive and maintains strong absorption performance under oblique incidence. The fabricated prototype demonstrates >90% absorption up to 75° for TE polarization and up to 60° for TM polarization. The structure is designed and optimized using CST Microwave Studio, with ML algorithms employed to predict absorption characteristics efficiently, reducing computational cost. The absorber is fabricated using a PCB process and validated through free-space measurements, showing strong agreement with simulations. The experimental results confirm the absorber's effectiveness for radar cross-section (RCS) reduction, EMI shielding, and sensing applications.

I. Introduction

Metamaterials are specifically engineered structures which are made to possess special electromagnetic properties that can't be realized in naturally present materials [1], [2], [3]. The materials have widely been investigated to be used for stealth technology, sensing, imaging, and wireless communication because of their capability of manipulating electromagnetic waves in unusual fashion [4], [5], [6]. Of the various metamaterial types, metamaterial absorbers (MMAs) have been an important research topic due to their high efficiency of absorption and capability to reduce unwanted electromagnetic interference. MMAs have applications in reducing radar cross-section (RCS), energy harvesting, biomedical imaging, and wireless security systems [7], [8], [9], [10]. But high-performance MMA design is difficult because of the requirement for fine adjustment of material properties and structural parameters to obtain broadband absorption under polarization and angle insensitivity [6], [11]. These approaches, although effective, are time and computationally intensive, especially when dealing with large parameter spaces. In a bid to bridge this gap, ML has emerged as a viable tool for optimizing the metamaterial design [12]. With data-driven approaches, ML can predict the electromagnetic response of MMAs without necessarily performing extensive simulations and thus conserving computational time and design time [13].

Various studies have investigated ML-based metamaterial design, but accuracy, generalizability, and fabricability limitations persist [14]. For example, the authors in [15] performed a comparative study of ML algorithms for MMA performance optimization and showed that ensemble learning algorithms like Extra Trees Regressor were superior to conventional optimization methods in estimating absorption properties. Nonetheless, their

work was specific to terahertz applications and did not cover wider frequency bands or fabrication limitations. Likewise, in [16] explored ML-aided reconfigurable antennas but did not generalize their method to broadband MMAs, confining their use to fixed-frequency devices.

The authors in [17], proposed a multi-layered design with enhanced angular stability but at the expense of increased fabrication complexity. Our absorber addresses such problems by reconciling absorptivity with fabrication viability to obtain high performance as well as a deployable design. The incorporation of ML into metamaterial design has been investigated further by researchers in terms of neural network-based optimization. But their model needed large amounts of training data, and that was not possible for rapid prototyping purposes [18]. Our work takes these advances a step further by using a hybrid paradigm in which ML is combined with parametric analysis to enable efficient optimization using very little training data. The hybrid approach will allow us to obtain better absorption properties without sacrificing computational efficiency [19], [20]. Aside from ML-based design, various research studies have also investigated new geometries and compositions of materials for MMAs. Yang et al. presented a novel broadband metamaterial absorber using textile based resistive film patterns [21]. Even though the design exhibits practical feasibility and flexibility, it does not employ ML for optimization. Similarly, Amiri et al. proposed a crescent-shaped resonator achieving over 99% absorption across various polarization angles [22]. However, the design emphasizes narrowband absorption and does not incorporate ML for optimization. This study addresses this limitation through the integration of a sophisticated ML-based optimization platform that guarantees high absorption performance across incident angles of different values [23].

In addition, it has been emphasized in recent studies that fabrication constraints play a crucial role in MMA design. The authors proposed in [24], a multi-layered design with enhanced angular stability but at the expense of increased fabrication complexity [25]. Likewise, Jing et al. introduced a surrogate-based method to design a metamaterial which even though was effective in optimization but lacked a focus on real world fabrication constraints [18]. Further, studies have focused on various design changes to enhance bandwidth. A few researchers have tried multi-layer stacking for bandwidth improvement, which can cause fabrication problems [24], [25], [26]. Electric field driven resonators for airborne radar applications were tried by others, resulting in greater absorption enhancement [27]. As a contrast, our design utilizes a single-layer manufacturing process while maintaining high absorption efficiency, thus being more viable for large-scale fabrication.

In addition, it has been emphasized in recent studies that fabrication constraints play a crucial role in MMA design. Wen et al. (2021) proposed a four-peaks absorption multi-layered structure in the range of 8–16 GHz, maximizing performance [25]. Yet, their design utilized multiple etching and deposition steps, which raises manufacturing complexity. As a contrast, our design utilizes a single-layer manufacturing process while maintaining high absorption efficiency, thus being more viable for large-scale fabrication.

In comparison to prior research, our work innovates the area by combining ML-optimized methods with real-world fabrication constraints. The MMA proposed in this paper has a number of significant enhancements over current designs:

1. Broadband Absorption – In contrast to narrowband MMAs that absorb only within small frequency bands, our design offers near-unity absorption over a broad frequency range. This is appropriate for applications in multi-band communications, radar stealth, and sensing technologies.
2. Machine Learning-Driven Optimization – Although past research has employed ML for metamaterial design, our method utilizes a hybrid ML model that incorporates artificial neural networks, decision trees, and gradient boosting methods. This allows for quicker and more precise optimization while minimizing computational expense.
3. Angle Insensitivity – Most current absorbers suffer from performance loss at off-normal incidence angles. Our work is designed to preserve high absorption efficiency at very large angles, hence making it more resilient for practical use.
4. Fabrication Feasibility – Multi-layered designs are prone to be complicated in mass-scale fabrication. Our MMA is optimized based on a single-layer structure with low fabrication complexity and ensuring scalability toward industrial applications.
5. Experimental Validation – In contrast to simulation-focused research, our research includes experimental validation through the production of prototypes. This allows us to confirm that our ML-optimized design is feasible and functions as expected.

By filling the gaps in the existing research and proposing a holistic ML-based optimization framework, this work considerably improves the design process for high-performance MMAs. The results show that ML-based methods not only enhance efficiency but also open up new avenues for customizing electromagnetic characteristics in metamaterial-based devices.

II. Design of proposed MMA

MMA developed in the present work includes a periodic configuration of resonator structures optimized for broadband absorption for a broad spectrum of frequencies. The unit cell is designed on an FR4 substrate having thickness of t_s, with a ground plane made of copper, as shown in Fig. 1(a). The top layer consists of a resonator designed in the shape of dual split-ring. After several iterations the unit cell MMA is realised with the given parameters, as shown in Fig. 1(b). The unit cell is arranged in a repetitive pattern to get the periodic arrangement of the MMA, as shown in Fig. 1(c). This is done to achieve the maximum absorptivity. Finally, the MMA is simulated with a set of boundary conditions, as shown in Fig. 1(d). Since the MMA has a metal back plane so the transmission is zero. The primary target of the design process is maximum absorption efficiency with angle insensitivity. To achieve this, geometrical configurations are investigated and fine-tuned as structural parameters are optimized using both numerical simulations as well as machine learning-based methods. Here, FR4 substrate is being considered for use, and the impact of it on the absorption efficiency is compared. To guarantee broadband absorption, the unit cell is subjected to repeated sweeps of parametric studies where key design parameters, such as the dimensions of the resonator and thickness of the substrate, are systematically changed. The frequency-dependent reflection coefficient (S_{11}) is computed with full-wave electromagnetic simulators CST Microwave Studio.

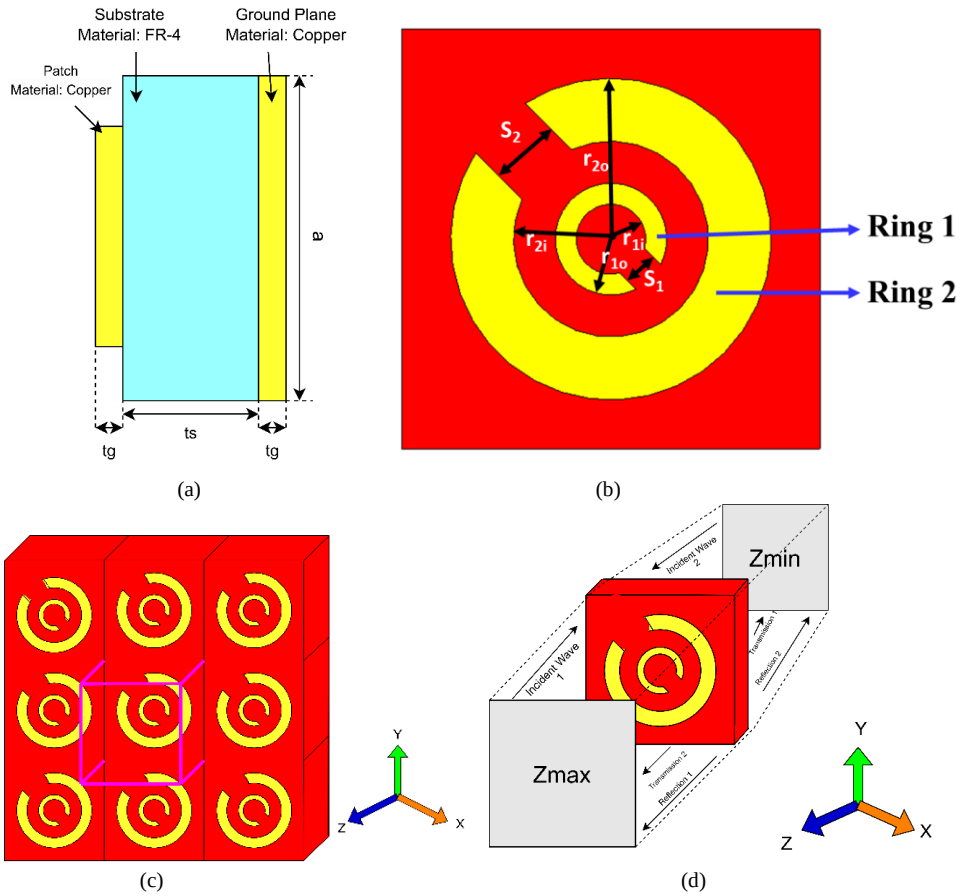

Fig. 1. (a) Design specifications of the MMA, (b) geometry of designed unit cell: detailed dimensions, (c) periodic arrangement of the unit cell, (d) simulation boundary conditions.

Table 1. Dimensions of the MMA.

Specification	Dimension (mm)	Description
a	6	Ground and substrate length and width
t_s	3	Substrate thickness
t_g	0.035	Ground thickness
r_{2o}	2.3	Ring 2 outer radius
r_{2i}	1.4	Ring 2 inner radius
r_{1o}	0.8	Ring 1 outer radius
r_{1i}	0.5	Ring 1 inner radius
S_2	1	Ring 2 split width
S_1	0.5	Ring 1 split width

The proposed MMA consists of two concentric split circular rings, referred to as Ring 1 and Ring 2, each having distinct inner and outer radii, denoted as r_{1i}, r_{1o} for Ring 1 and r_{2i}, r_{2o} for Ring 2. The rings are symmetrically arranged on the dielectric substrate and feature split gaps of widths S_1 and S_2, which play a crucial role in tailoring the electromagnetic response of the structure. These split gaps introduce capacitive effects, influencing the resonance characteristics and enhancing absorption efficiency. The optimized geometric parameters ensure strong interaction with incident electromagnetic waves, leading to efficient absorption over a broad frequency range. All the dimensions are shown in Table 1.

III. Evolution of Proposed MMA

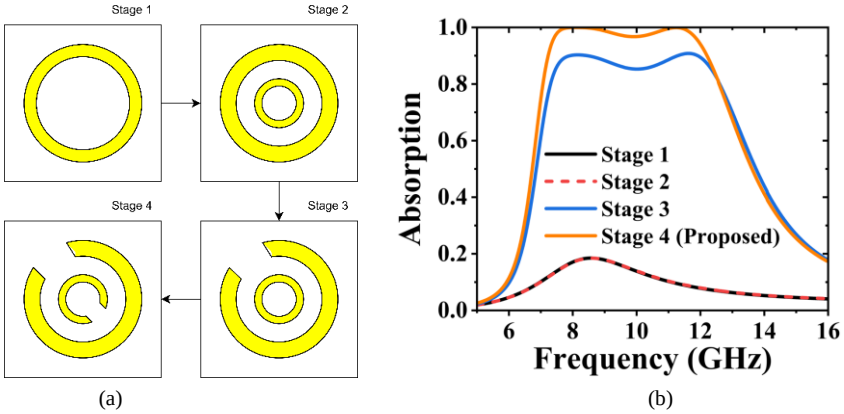

Fig. 2. (a) Development of proposed absorber, and (b) Absorption.

The first step in the design is to choose an effective unit cell structure as the basic building element of the MMA. The geometry of the unit cell comprises a patterned metal resonator on a dielectric substrate and a metal ground plane on the back side to prevent transmission. The resonator shape plays an important role in the absorption performance, and various geometries like circular rings, split-ring resonators, and cross-wire geometries are explored. After several stages of design, the final split-ring design is achieved, as illustrated in Fig. 2(a). Fig. 2(b) illustrates the absorptivity results at different stages of the design process. The plot shows that the best absorptivity result is achieved for stages 3 and 4. The stage 4 which is the proposed configuration gives a better absorption of >90% from 7.13-12.22 GHz with bandwidth of 5.09 GHz with fractional bandwidth of 52.60 %.

IV. Stability

The stability of the proposed MMA is investigated under both Transverse Electric (TE) and Transverse Magnetic (TM) wave incidences as depicted in Fig. 3. In TE incidence, the electric field is perpendicular to the plane of incidence, while the magnetic field has both normal and parallel components. In TM incidence, the magnetic field is perpendicular to the plane of incidence, while the electric field has both normal and parallel components.

It can be observed that the proposed MMA exhibits an identical response for both TE and TM polarizations, demonstrating its polarization-insensitive nature. This stability is crucial for ensuring consistent performance in practical applications. The near-identical absorption characteristics under TE and TM incidences indicate that the structure maintains its effectiveness regardless of the polarization of the incident wave, making it highly suitable for real-world applications where polarization variations are common. Moreover, the proposed absorber is investigated for TE, and TM modes under various incidence angles (θ). The proposed absorber maintains over 80% absorption for TE incidence up to 75°, indicating strong polarization-insensitive behaviour as depicted in Fig. 3(b). The absorber maintains absorption > 80% for TM incidence up to 60°, demonstrating good angular stability as depicted in Fig. 3(c). However, the performance is slightly reduced compared to TE incidence due to different field interactions with the structure. The angular dependence of absorption is influenced by

impedance matching, resonator geometry, and field distribution. These factors contribute to the wide-angle absorption capability of the proposed design, making it highly suitable for practical applications.

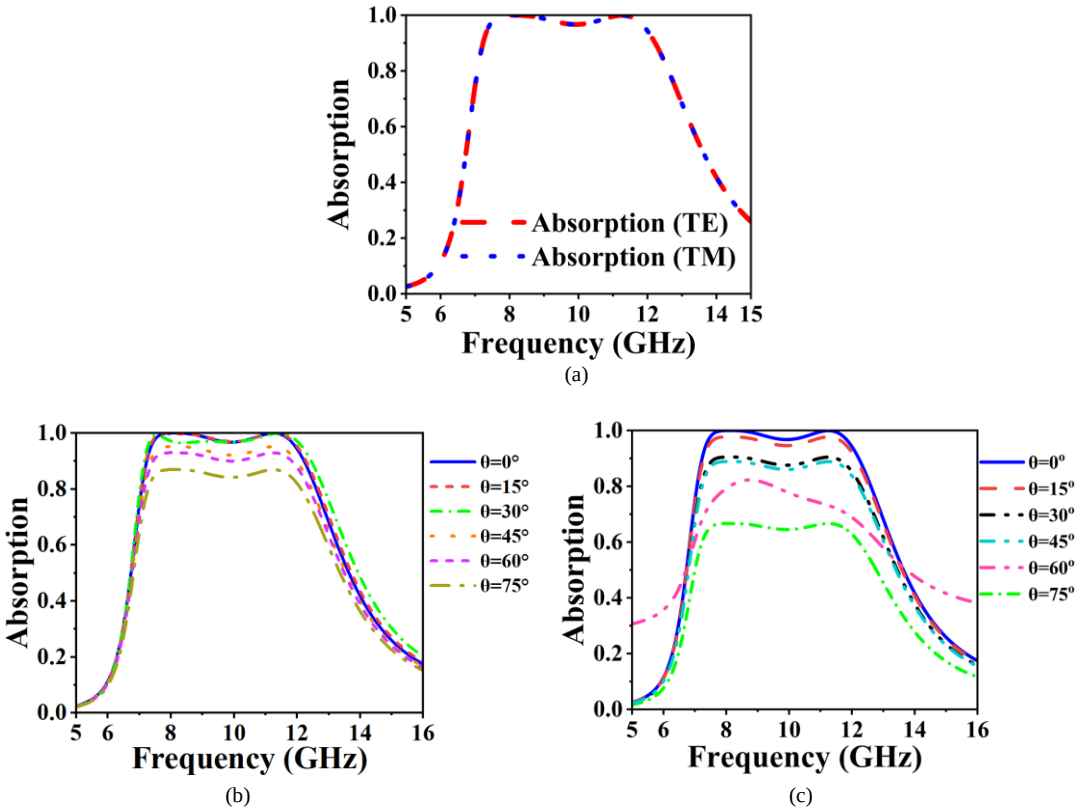

(a) (b) (c)

Fig. 3. Absorption plot: (a) TE polarization and TM polarization. Under various θ: (b) TE, and (c) TM modes.

V. Parametric Analysis

The proposed metamaterial absorber (MMA) is investigated for the variation of different physical parameters to analyze its impact on absorption performance. The key parameters considered include the thickness of the substrate (t_s), the inner and outer radius of Ring 1, and Ring 2 (r_{1o}, r_{1i}, r_{2o}, r_{2i}), split gaps (S_1, S_2).

Initially, the thickness of the substrate (t_s) is varied from 2 mm to 4 mm in steps of 0.5 mm, as depicted in Fig. 4(a). It is observed that for ts=3 mm, the absorber exhibits wideband absorption ranging from 7.13 GHz to 12.22 GHz. However, for other values of t_s, the absorber's performance deteriorates. This deterioration is due to impedance mismatch between the absorber and free space, affecting absorption efficiency. Deviations in substrate thickness shift resonance conditions, leading to reduced absorption and increased reflection by altering the structure's effective permittivity and permeability. Next, the inner and outer radii of Ring 2 (r_{2i}, r_{2o}) are investigated as shown in Fig. 4(b), and Fig. 4(c). For r_{2i} = 1.5 mm and r_{2o} = 2.6 mm, the absorber exhibits wideband absorption. Additionally, for r_{2i} = 1.2 mm and 1.8 mm, the absorber maintains absorption above 90%. However, for other values of r_{2o}, the absorber fails to achieve wideband performance. The optimal values of r_{2i}, and r_{2o} ensure proper resonance coupling, leading to wideband absorption. Deviations from these values disturb the electromagnetic field distribution, causing impedance mismatch and reduced bandwidth.

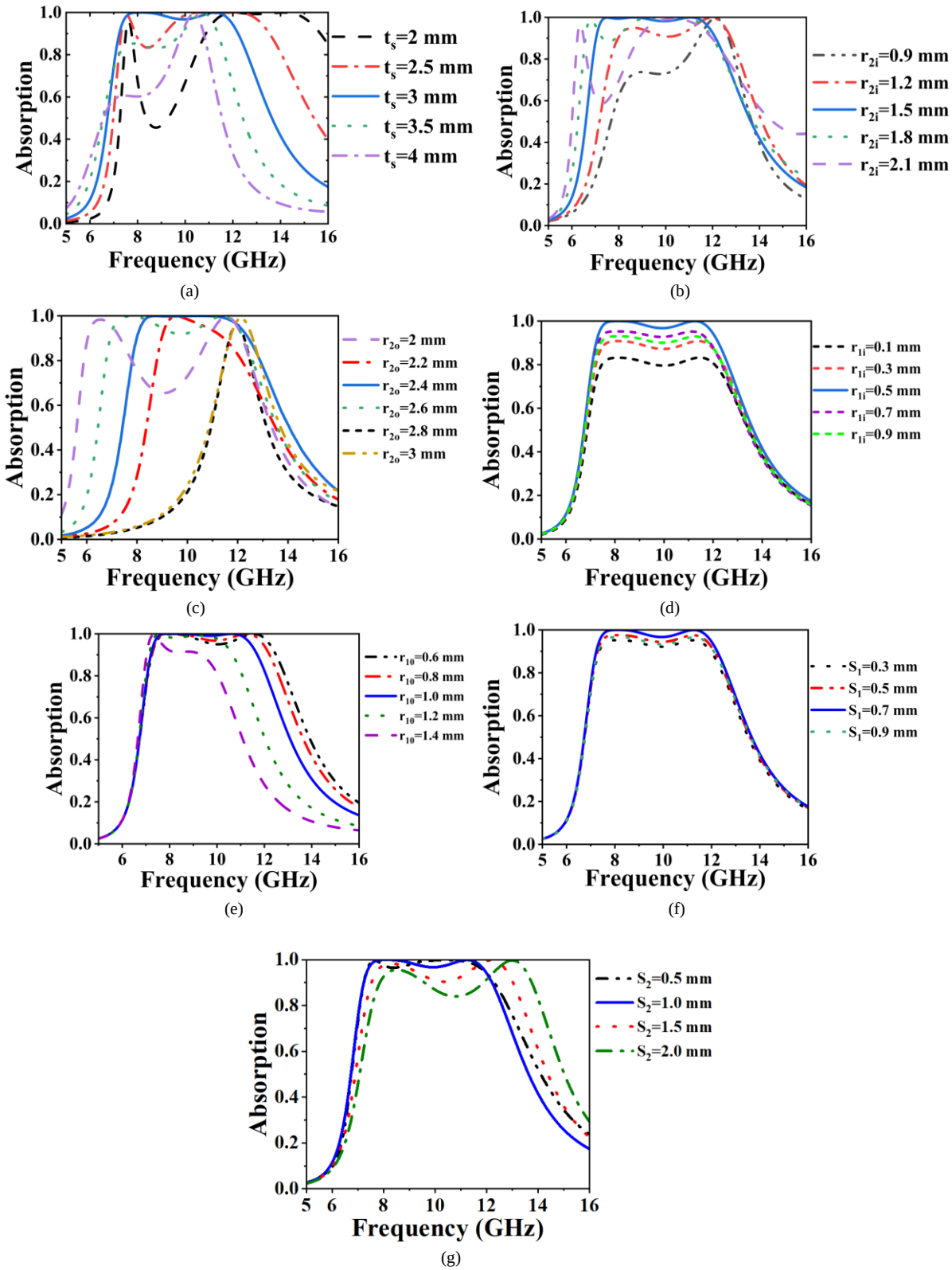

Fig. 4. Parametric analysis results for different (a) Substrate thickness, (b) r_{2i}, (c) r_{2o}, (d) r_{1i}, (e) r_{1o}, (f) bigger ring split width, and (g) smaller ring split width.

Similarly, the r_{1i}, r_{1o} are varied as depicted in Fig. 4(d) and Fig. 4(e). The optimum values are r_{1i} = 0.5 mm and r_{1o} = 1 mm, where the absorber exhibits wideband performance. For all values of r_{1i}, the absorber maintains absorption greater than 80%. Furthermore, for different values of r_{1o}, the absorber achieves over 90% absorption, except for r_{1o} = 1.4 mm, where it

shows narrowband absorption. This behaviour occurs because the dimensions of Ring 1 significantly influence the resonance modes and field distribution. Deviations from the optimal values alter the coupling between resonators, leading to impedance mismatch and reduced bandwidth. In particular, for r_{1o} = 1.4 mm, the resonance shifts, limiting the broadband response and resulting in narrowband absorption.

Additionally, the split gaps of Ring 1 and Ring 2 (S_1, S_2) are investigated. For all values of S1, the absorber maintains wideband performance, but for S_1 = 0.7 mm, it shows better absorption compared to other values. Similarly, for S_2 = 1 mm, the absorber exhibits excellent wideband absorption and maintains greater than 90% absorption for other values as well. The split gaps influence the capacitive coupling and electric field distribution, affecting resonance behaviour. The optimized values of S_1 and S_2 enhance electromagnetic wave trapping, improving absorption efficiency. However, deviations can lead to slight impedance mismatches, impacting overall absorption performance.

VI. Machine Learning Model Training

The traditional method of designing MMAs is based on time-consuming numerical simulations, demanding large computational resources to scan through large design parameter spaces. To circumvent these limitations, we incorporate machine learning into the design process, allowing for effective prediction of absorber performance without exhaustive simulations. A dataset is created by varying system parameters like resonator dimensions, substrate thickness and material properties in a controlled manner while measuring the respective absorption characteristics. From the parametric analysis defined in section IV it can be observed that the maximum absorptivity is achieved at for t_s = 3 mm, and width of 6 mm. From the parametric analysis, with the maximum absorptivity observed at the optimized parameters shown in Table 1. This dataset is utilized to train several ML models to predict the absorption response for new, unseen configurations.

Data Pre-processing

Prior to training the ML models the dataset goes through pre-processing for high-quality input data. Steps involved are:

1. Normalization: Because the design parameters consist of different numerical ranges, feature scaling is utilized for normalizing them in a way that all input values lie on the same scale.
2. Feature Selection: Variables that are redundant and highly correlated are dropped to enhance model efficiency and prevent overfitting.
3. Data Augmentation: Synthetic data points are created in addition to the available data using interpolation methods to enhance the dataset and model generalization.
4. Splitting the Dataset: The dataset is split into training (80%), validation (10%), and testing (10%) subsets for measuring model performance.

Model Selection and Training

A number of machine learning models are tested to identify the most efficient strategy for predicting metamaterial absorption properties:

1. Artificial Neural Networks: Multi-layer perceptron's with nonlinear activation functions are utilized to learn intricate relations between input parameters and absorption values. The network has more than one hidden layer with dropout regularization to avoid overfitting.
2. Random Forest Regressor: A decision-tree-based ensemble learning model that is capable of capturing interactions between design parameters and making strong predictions.
3. Gradient Boosting Algorithms: XGBoost and LightGBM are used to enhance prediction precision by iteratively minimizing error in sequential training iterations.
4. Support Vector Regression (SVR): A kernel-based learning algorithm that transforms input parameters into absorption properties using high-dimensional mappings.

Fig. 5 shows how computational cost increases with model complexity. Even though complex models have more training cost index but they generalize better.

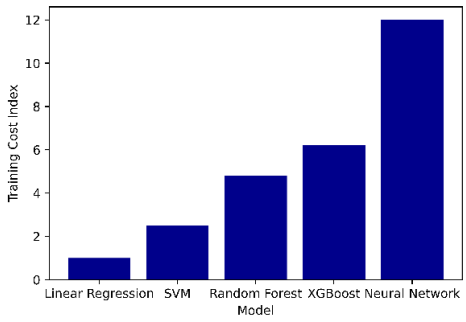

Fig. 5. Computational cost vs. Model complexity.

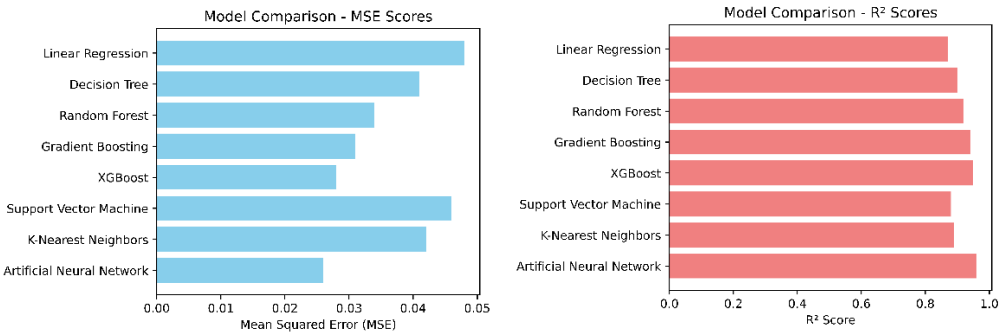

Fig. 6. (a) Model MSE comparison and (b) R^2 comparison.

Each model is hyperparameter tuned with grid search and Bayesian optimization methods to determine the best configurations that optimize predictive performance. The models are ranked on mean squared error (MSE) and R-squared (R^2) metrics, as shown in Fig. 6 (a), and Fig. 6(b). The top-performing model is chosen for the optimization platform. Feature importance analysis is also performed to determine which design parameters have the greatest impact on absorption performance. After training the ML model, it is incorporated into an optimization platform that forecasts the optimal design parameters to achieve maximum absorption. The process of optimization is multi-stage in nature.

Regression-Based Optimization

The trained ML model is used as a surrogate function that mimics the relation between design parameters and absorption features. Rather than executing full-wave simulations for each combination of parameters, the ML model quickly estimates absorption values to enable efficient optimization.

A multi-objective optimization problem is set where the objective function aims to:

1. Maximize the efficiency of absorption within the target frequency band.
2. Minimize incidence-angle dependence.
3. Minimize fabrication complexity with high performance.

The optimization method continually optimizes design parameters using the ML model to forecast absorption behaviour until a suitable configuration is attained.

Comparison with Traditional Methods

The performance of the ML-based optimization framework is verified through comparison with traditional simulation-driven optimization methods. The traditional methods need hundreds of simulations to optimize design parameters while the ML-based approach yields comparable or better performance with much lower computational resources. The design thus obtained by ML optimization is then again simulated with full-wave simulations in order to ensure accuracy. The final design that is chosen must be able to provide broadband absorption and angle insensitivity and ease of manufacturing. One of the greatest contributions this research can do is to be able to implement ML methods within the design process of MMAs. The conventional method of design for metamaterials is through the use of a trial-and-error simulation process. This is obviously computationally expensive and time-consuming. We thus had a much more efficient, systematic optimization process with the predictive modelling of the ML-based models.

Model	MSE	R^2 Score
Linear Regression	0.048	0.87
Decision Tree	0.041	0.90
Random Forest	0.034	0.92
Gradient Boosting	0.031	0.94
XGBoost	0.028	0.95
Support Vector Machine	0.046	0.88
K-Nearest Neighbours	0.042	0.89
Artificial Neural Network (ANN)	0.026	0.96

Table 3. ML Model Comparison

The ML models used in this study like artificial neural networks and ensemble learning techniques allowed rapid prediction of absorption characteristics for different design configurations. This enabled us to search through a much bigger design space in a fraction of the time taken by traditional methods. Table 3 shows the comparison of different ML models based on their MSE scores and their R^2 scores. The table clearly shows that ANN performed the best among all the different models used for this study.

Yet another advantage of optimization using ML is that it may identify subtle interactions between design parameters that are hard to identify by traditional analysis. Feature importance analysis revealed critical parameters with the highest impact on absorption performance, which allowed us to focus optimization efforts on these dominant factors. Focused optimization kept

computational overhead at a minimum while maximizing the effectiveness of the optimized design. The framework of ML that has been developed in this work can be used to extend to other metamaterial structures like antennas, frequency-selective surfaces and electromagnetic shielding devices. The versatility of ML-based optimization makes it a valuable tool for future studies on metamaterials.

VII. Filed Analysis

The Electric field (E), Magnetic field (H), and surface current distribution on the proposed absorber is analyzed for wide band absorption. The strong electric and magnetic resonances observed in Fig. 7 are responsible for the enhanced broadband absorption.

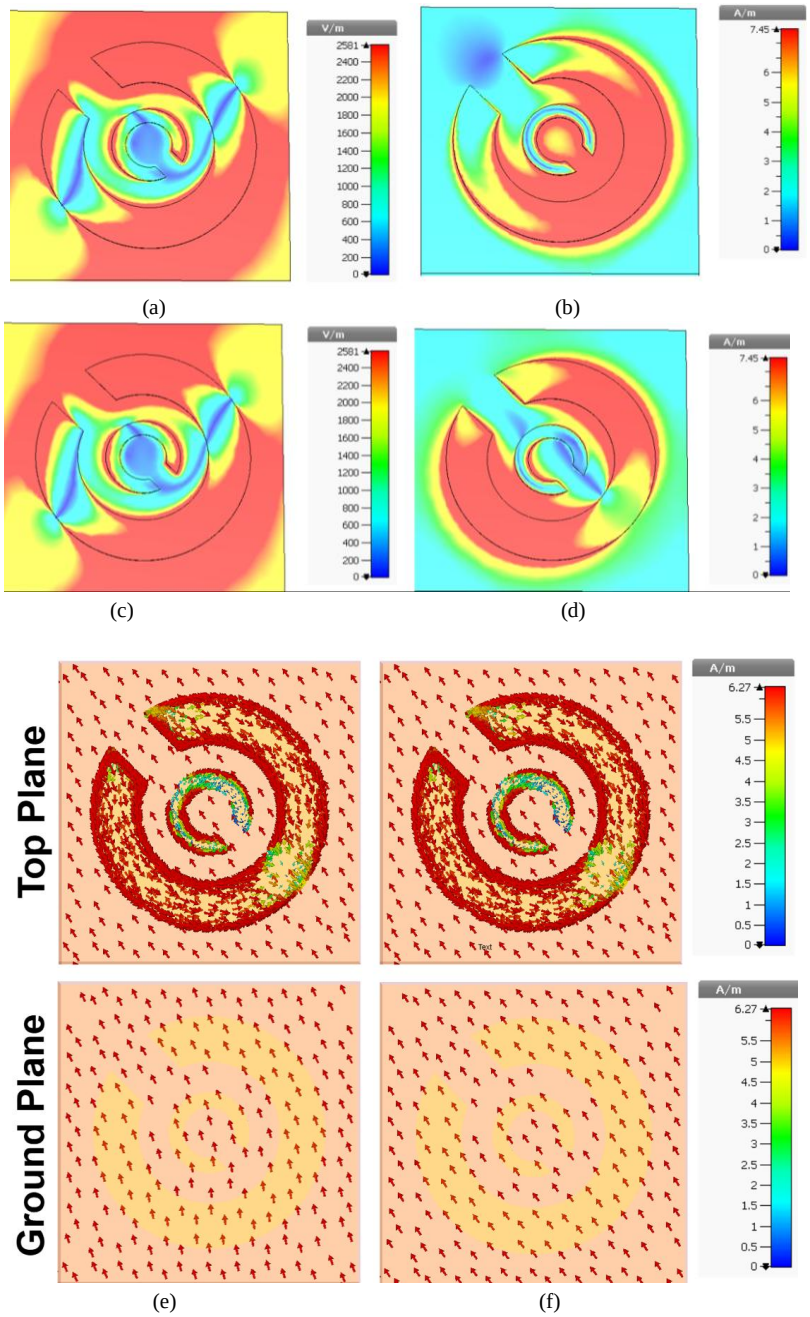

Fig. 7. The E distribution at (a) 8.2 GHz, (c) 11.2 GHz. H distribution at (b) 8.2 GHz, (d) 11.2 GHz and surface current distribution at (e) 8.2 GHz and (f) 11.2 GHz.

The electric field distribution at 8.2 GHz (Fig. 7a) and 11.2 GHz (Fig. 7c) shows strong field localization around the split gaps of the resonators. At these resonance frequencies, the electric field is highly concentrated in these regions due to charge accumulation and capacitive coupling, which plays a crucial role in absorption. The intense E-field at the gaps indicates strong dipole-like resonance behaviour, contributing to enhanced energy confinement and absorption. Additionally, the field distribution confirms that resonance modes are efficiently excited at the designed frequencies. Additionally, the magnetic field distribution at 8.2 GHz (Fig. 7b) and 11.2 GHz (Fig. 7d) exhibits strong field enhancement around the circular rings, particularly in the inner and outer edges of the resonators. The H-field is primarily concentrated in the dielectric substrate, demonstrating strong magnetic dipole interaction, which is essential for impedance matching with free space. The effective magnetic response, combined with the electric field interaction, ensures the efficient trapping of incident electromagnetic waves, leading to near-perfect absorption at the resonance frequencies.

The surface current distribution is analyzed for both the top meta-structure and the ground plane at 8.2 GHz (Fig. 7e) and 11.2 GHz (Fig. 7f). The results indicate that at both resonance frequencies, strong circulating currents are observed on the top metallic resonators, particularly along the edges of the split-ring structures. These circulating currents generate a magnetic dipole effect, which enhances the absorption performance by inducing strong electromagnetic coupling. The ground plane current distribution shows a relatively uniform but opposing pattern, ensuring minimal reflection and maximum absorption. The presence of anti-parallel currents between the top and bottom layers signifies the formation of magnetic resonance, which is a key mechanism in metamaterial absorbers.

VIII. Fabrication and Experimental Setup

The proposed metamaterial absorber consists of two split circular rings patterned on a dielectric substrate with a metallic ground plane. The fabrication process begins with the selection of a low-loss dielectric substrate (e.g., FR-4, Rogers RT/Duroid) with a thickness of ts mm. The substrate is thoroughly cleaned to remove any surface contaminants and ensure proper adhesion of conductive layers. A thin copper layer (~35 μm) is laminated on both sides of the substrate. The top layer is patterned with the designed two split circular rings using standard photolithography and chemical etching techniques. A photoresist is applied, exposed to UV light through a mask, and developed to define the metamaterial structure. The unwanted copper is then removed using wet chemical etching, leaving behind the precise pattern of the resonators. The bottom layer remains as a continuous copper ground plane, ensuring minimal transmission and maximum absorption. After etching, the fabricated structure is cleaned to remove any residual chemicals. A high-resolution optical microscope and scanning electron microscope (SEM) are used to inspect the structure and verify fabrication accuracy. Additionally, surface roughness and conductivity measurements are performed to ensure fabrication quality. Finally, the fabricated absorber is tested using a vector network analyzer (VNA) in an anechoic chamber to measure the absorption characteristics under normal and oblique incidence. These experimental results are compared with simulation data to validate the absorber's performance. This fabrication process ensures high precision and efficiency, making the metamaterial absorber suitable for practical applications.

Fig. 8 shows the fabricated MMA. The fabricated array structure is of 40 mm x 40 mm size. The compact design is one of the biggest advantages of the proposed MMA design which is able to achieve high absorptivity with compact size.

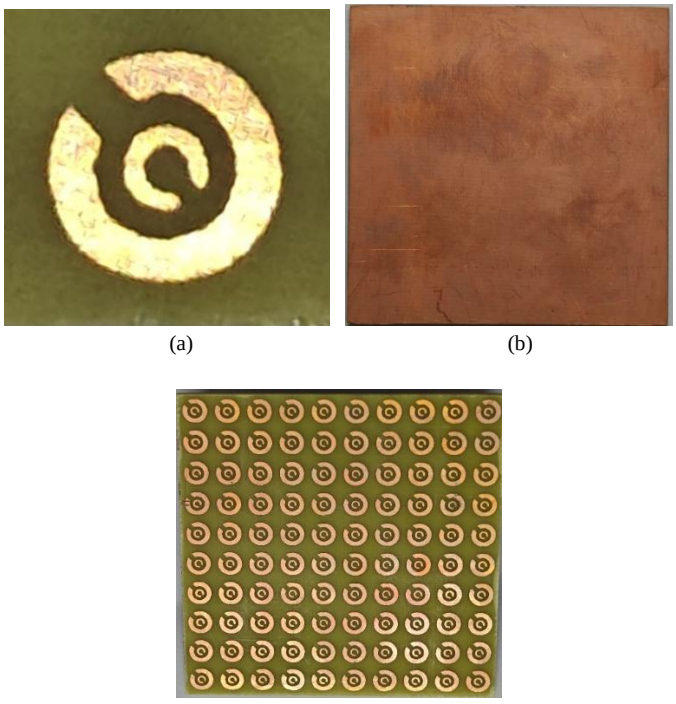

(a) (b)

(c)

Fig. 8. Fabricated MMA (a) unit cell, (b) back view, and (c) periodic arrangement front view.

The optimized MMA was first studied using full-wave electromagnetic simulations based on CST Microwave Studio. The main objective was to assess its absorption properties over an extensive frequency range and confirm its efficiency under various circumstances. Near-unity absorption was shown in the results. The performance was remarkably better than in conventional MMA designs, which tend to experience narrow bandwidth constraints. In order to further prove the efficacy of the designed absorber, different oblique incidence angles have been tested. The results in simulations confirmed that the absorber achieves stable absorption performance for angles of up to 45°, proving its resilience in actual applications where wave incidence can be unpredictable. Most traditional absorbers have poor performance at high incident angles owing to impedance mismatches, but our design does away with these problems by utilizing machine learning (ML)-tuned structural parameters.

The design was compared to current MMAs using a comparative study to provide benchmarking for our design performance. The results of the study were that our ML-optimized absorber demonstrated larger absorption and higher efficiency compared to past works utilizing heuristic-based design methodologies. The major performance characteristics, including the absorption bandwidth and angular stability were all drastically improved.

After simulation-based optimization, a absorber prototype was fabricated and tested experimentally. Fabrication involved photolithography and etching processes to transfer the resonator patterns onto a dielectric substrate. The test of the fabricated prototype was carried out with a vector network analyser (VNA) and standard horn antennas to characterize the reflection and transmission coefficients. Fig. 9 presents the simulated and measured results for

S11 (dB) and absorptivity across the operating frequency range. Fig. 9(a) illustrates the S11 (dB) plots for both simulation and measurement, showing close agreement, which validates the accuracy of the fabrication process and the reliability of the proposed absorber. One of the most important components of experimental verification was the demonstration of the absorber's operation at various different polarization angles. The absorption plots in Fig. 9(b) and Fig. 9(c) under TE and TM polarization angles exhibit a close correlation between numerical and experimental values, further confirming the effectiveness of the ML-based optimization process. Minor discrepancies observed between the simulated and measured results are primarily due to fabrication tolerances and material property variations. However, these variations remain within acceptable limits and do not significantly impact the overall absorption performance. This demonstrates that the proposed absorber is a strong candidate for electromagnetic shielding, stealth technology, radar cross-section (RCS) reduction, and sensing applications due to its high absorption performance and stability under varying conditions.

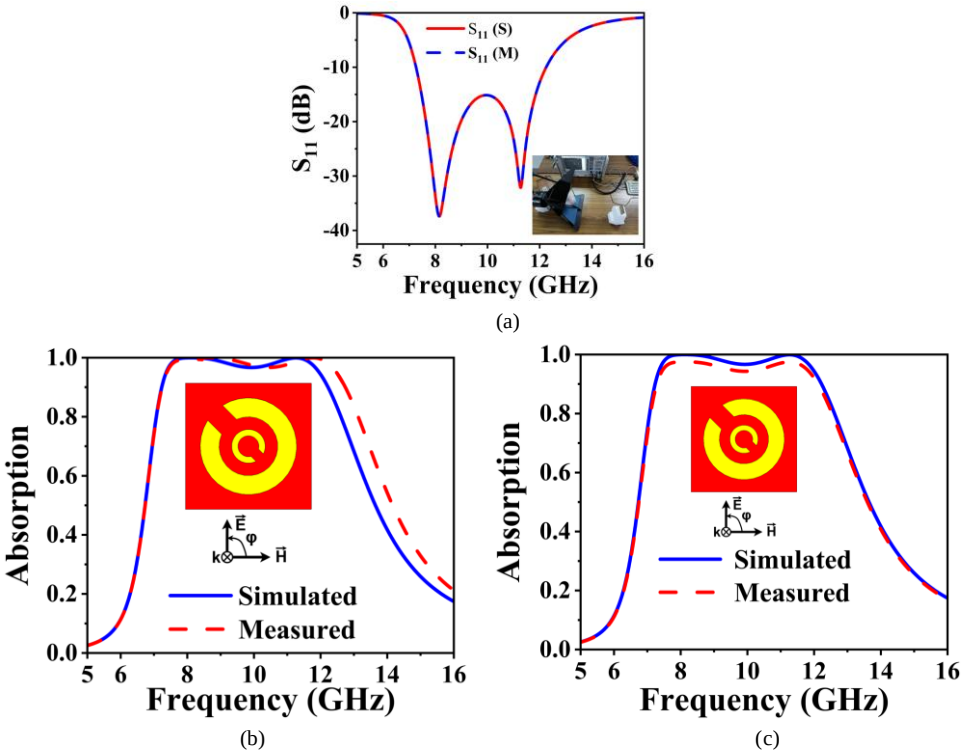

Fig. 9. Simulations and measurement results of the proposed MMA: (a) S_{11} (dB), and for various polarization angles (φ), (b) TE Incidence, and (c) TM incidence.

Moreover, Fig. 10 shows the comparison between simulated and measured absorptivity at different incidence angles under TE and TM incidence. The findings validated that the designed absorber maintains its high absorption rate even at large angles, an important benefit compared to traditional absorbers whose performance degrades when exposed to oblique incidence. This angle independence is very important in stealth and sensing applications where the direction of incident electromagnetic waves is not predetermined.

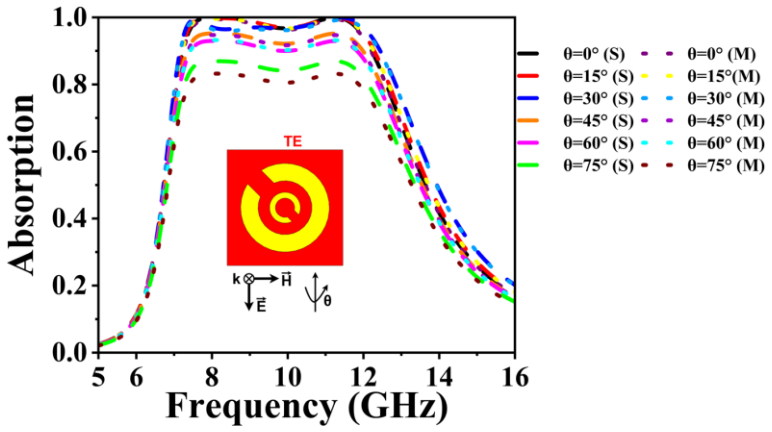

(a)

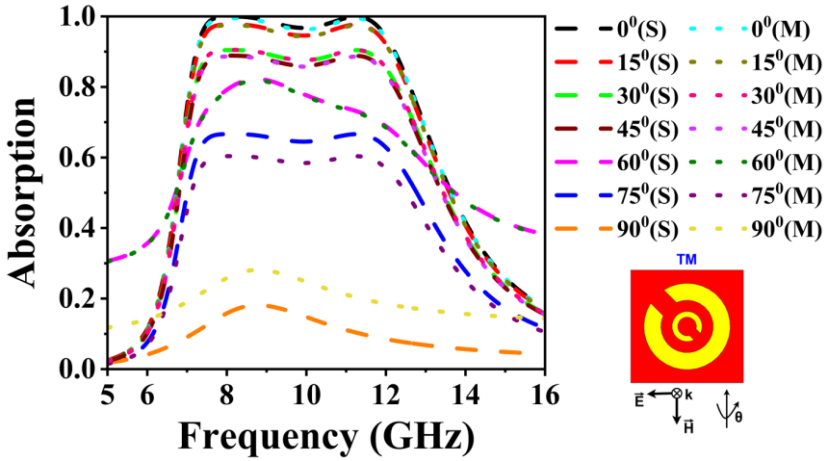

(b)

Fig. 10. Simulation and measurement of absorption for different values of θ under (a) TE, and (b) TM.

IX. EM Shielding

The proposed absorber is investigated for EM shielding. This broadband absorber, with its high absorption capability, fulfils the essential requirements for EMI shielding and stealth applications. The shielding performance is evaluated using Shielding Effectiveness (SE), which is determined by key factors such as Absorption Shielding Effectiveness (SEA), Reflection Shielding Effectiveness (SER), and Multiple Reflection Shielding Effectiveness (SEMR). SE measures the ability of a material to attenuate electromagnetic waves, playing a crucial role in reducing EM interference. The following equations are used to compute these components:

$$SE = SEA + SER + SEMR \quad (1)$$

$$SEA = -10 \times \log_{10}(TC/1 - RC) \quad (2)$$

$$SER = -10 \times \log_{10} \frac{1}{RC} \quad (3)$$

$$SEMR = -10 \times \log_{10}(1 - RC^2) \quad (4)$$

Here TC, and RC are transmission and Reflection Coefficient. Fig. 11 depicts the SEA, and SER for the proposed absorber. The SEA value remains consistently above 40 dB within the operating frequency range and which can be enhanced by improving the reflector thickness. A minimum SEA of 10 dB is generally sufficient to minimize the influence of multiple

reflections. Moreover, the SER result is negligible, staying < 1 dB, demonstrating that the absorber efficiently confines the incident electromagnetic wave energy.

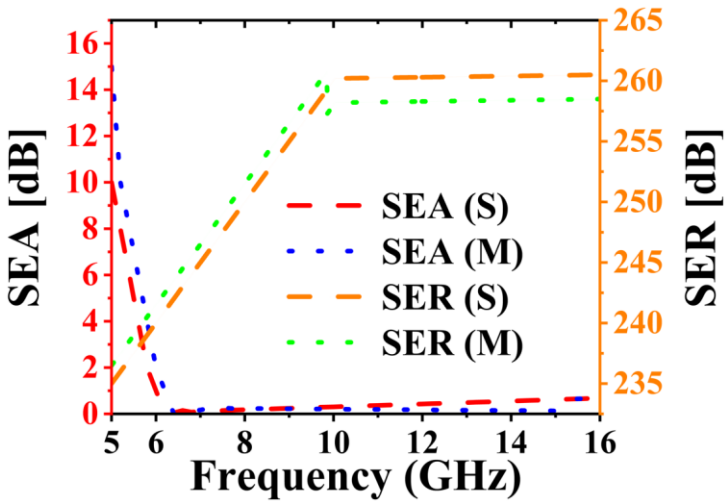

Fig. 11. Shielding Effectiveness: SEA (dB), and SER (dB).

X. Comparison with Existing Designs

To emphasize the achievements made in this research, a thorough comparison with existing MMA designs was carried out. A number of performance indicators were utilized for this comparison, and they are:

1. Absorption Bandwidth: The ML optimized design had a wider absorption bandwidth compared to conventional absorbers. Most of the earlier research considered narrowband absorbers that only operated in a specific narrow frequency range and while our design has near unity absorption in a relatively much wider spectrum.
2. Computational Efficiency: The optimization technique driven by ML minimized the number of simulations needed as opposed to traditional heuristic-based methods. Computational efficiency was attained through the use of predictive modelling to influence parameter selection, thus cutting down on computation time.
3. Fabrication Complexity: In contrast to some multi-layer absorbers that involve complicated fabrication processes, our design is more flexible when it comes to industrial production.
4. Angle Insensitivity: The majority of previous designs suffer from performance deterioration with varying polarization state and incidence angle. Our absorber has high efficiency under different polarization conditions and up to 45° incidence angle and which makes it more stable for real-world usage.

Table 3 shows the proposed MMA characteristics compared with the published literature characteristics. These comparisons identify the merits of the proposed ML optimized MMA and demonstrate its potential for widespread utilization in state-of-the-art electromagnetic applications.

Table 3. Benchmarking with prior research.

Ref.	F- band	Dimension (mm)	t_s (mm)	BW (GHz)	Substrate layer composition	Angular stability of >90% absorption
[11]	Ku-band	39 (1.95λ_o)	1.6(0.08λ_o)	1.98(13.33%)	Single	45° (TE, TM)
[23]	C- and X-band	20 (0.621λ_o)	3.2(0.1λ_o)	1.86(20.6%)	Two	45° (TE, TM)
[25]	X- and Ku-band	18 (0.626λ_o)	0.69(0.024λ_o)	-	Two	-
[26]	C-band	13.25 (0.249λ_o)	1(0.096λ_o)	0.42(4.65%)	Single	60° (TE), 30° (TM)
[28]	X-band	10 (0.346λ_o)	1(0.034λ_o)	0.68(6.55%)	Single	45° (TE), 30° (TM)
[27]	C-, X-, Ku- and K-band	6.6 (0.308λ_o)	3.7(0.173λ_o)	12(85.7%)	Four	45° (TE), 15° (TM)
Proposed work	X-band	6 (0.162λ_o)	3(0.081λ_o)	5.37 (54.71%)	Single	75° (TE, TM)

Ref: Reference, F: Frequency, BW: Bandwidth

XI. Conclusion

This study shows the applicative possibility of machine learning (ML) for providing an optimized design of high-performance MMAs, achieving broadband absorption with insensitivity to incidence angles. By integrating ML techniques with traditional simulation methods, the design process was significantly accelerated, reducing computational costs while enhancing absorber performance. The proposed framework utilized artificial neural networks (ANNs) and ensemble learning models to predict absorption characteristics, enabling efficient exploration of design parameters. The experimental verification showed that the ML-optimized absorber and the simulation results matched closely. The minimal discrepancies observed were attributed to fabrication tolerances and measurement uncertainties, further emphasizing the practical viability of ML-driven optimization. Compared to traditional heuristic-based methods, the ML approach offered faster convergence to optimal designs while maintaining superior absorption performance.

Contrary to existing studies that have focused excessively on iterative simulations this research incorporated ML behind the scenes throughout the process of real-time optimization of the different absorber parameters. The results underscore the potential of ML in metamaterial research, offering a scalable and efficient alternative to computationally intensive optimization techniques. The methodology presented here can be extended to other electromagnetic applications, including reconfigurable antennas, electromagnetic shielding, and wavefront engineering. Future research can examine deep learning-based generative design models for further automating the process of optimization. The increase in the number of material and fabrication constraints included in the datasets can further improve the model's ability to generalize. With developing ML techniques, their practicality in engineering metamaterials will help boost advancements in high-performance electromagnetic wave manipulation.

Credit authorship contribution statement: **Himanshu Shekhar, Gauri Ojha, Pranav Gupta, Upender Patri**: Research, Writing – review, Validation, funding.

Declaration of Competing Interest The authors of the manuscript hereby declare that the above manuscript which is submitted for publication in this journal is NOT under consideration elsewhere. The manuscript is NOT published already in part or whole in any journal or

magazine for private or public circulation. The manuscript does not violate the intellectual property rights of any third party. All the named authors have no conflicts of interest to disclose.

Acknowledgement: The work was supported by Vellore Institute of Chennai, Tamil Nadu, INDIA.

References

[1] P. Upender, S. P. Bharathi, Sukriti, K. Kumba, and A. Kumar, "A Compact Metamaterial Biosensor for Multi-Virus Detection With Tunability and High Incidence Angle Absorption," *IEEE Access*, vol. 11, pp. 131915–131925, 2023, doi: 10.1109/ACCESS.2023.3336815.

[2] P. Upender and A. Kumar, "Ultrathin, Ultra Narrow Band DMMA for Biosensing Applications," *IEEE Trans Nanobioscience*, vol. 22, no. 3, pp. 529–537, Jul. 2023, doi: 10.1109/TNB.2022.3217077.

[3] S. Feng, Y. Zhao, and Y. L. Liao, "Dual-band dielectric metamaterial absorber and sensing applications," *Results Phys*, vol. 18, p. 103272, Sep. 2020, doi: 10.1016/J.RINP.2020.103272.

[4] H. Liu, Z. H. Wang, L. Li, Y. X. Fan, and Z. Y. Tao, "Vanadium dioxide-assisted broadband tunable terahertz metamaterial absorber," *Scientific Reports 2019 9:1*, vol. 9, no. 1, pp. 1–10, Apr. 2019, doi: 10.1038/s41598-019-42293-9.

[5] G. Wang, F. Zhu, T. Lang, J. Liu, Z. Hong, and J. Qin, "All-metal terahertz metamaterial biosensor for protein detection," *Nanoscale Res Lett*, vol. 16, no. 1, pp. 1–10, Jun. 2021, doi: 10.1186/S11671-021-03566-3/TABLES/2.

[6] P. Jain *et al.*, "Machine Learning Techniques for Predicting Metamaterial Microwave Absorption Performance: A Comparison," *IEEE Access*, vol. 11, pp. 128774–128783, 2023, doi: 10.1109/ACCESS.2023.3332731.

[7] P. Jain *et al.*, "Machine learning assisted hepta band THz metamaterial absorber for biomedical applications," *Scientific Reports 2023 13:1*, vol. 13, no. 1, pp. 1–12, Jan. 2023, doi: 10.1038/s41598-023-29024-x.

[8] M. A. Haque *et al.*, "Machine learning-based technique for gain and resonance prediction of mid band 5G Yagi antenna," *Scientific Reports 2023 13:1*, vol. 13, no. 1, pp. 1–22, Aug. 2023, doi: 10.1038/s41598-023-39730-1.

[9] K. Aliqab, B. B. Han, O. P. Kumar, M. Alsharari, A. Armghan, and S. K. Patel, "Graphene metamaterial solar absorber using Al-TiN-Fe for efficient solar thermal energy conversion and optimization using machine learning," *Scientific Reports 2024 14:1*, vol. 14, no. 1, pp. 1–14, Dec. 2024, doi: 10.1038/s41598-024-80485-0.

[10] R. Gadhafi *et al.*, "Exploring the Potential of Deep-learning and Machine-learning in Dual-band Antenna Design," *IEEE Open Journal of the Computer Society*, 2024, doi: 10.1109/OJCS.2024.3463190.

[11] M. J. Uddin, M. H. Ullah, and S. Z. Islam, "A Broadband Polarized Metamaterial Absorber Driven by Strong Insensitivity and Proximity Effects," *IEEE Access*, vol. 9, pp. 131672–131684, 2021, doi: 10.1109/ACCESS.2021.3114164.

[12] M. Yusuf, N. D. Bhandare, A. Sahaya Anselin Nisha, and S. Roy, "A Machine Learning Based Design of Frequency Reconfigurable Compact Microstrip Patch Antenna," *2023 IEEE Microwaves, Antennas, and Propagation Conference, MAPCON 2023*, 2023, doi: 10.1109/MAPCON58678.2023.10463931.

[13] G. Cerniauskas, H. Sadia, and P. Alam, "Machine intelligence in metamaterials design: a review," *Oxford Open Materials Science*, vol. 4, no. 1, Jan. 2024, doi: 10.1093/OXFMAT/ITAE001.

[14] P. Jain *et al.*, "Multiband Metamaterial absorber with absorption prediction by assisted machine learning," *Mater Chem Phys*, vol. 307, p. 128180, Oct. 2023, doi: 10.1016/J.MATCHEMPHYS.2023.128180.

[15] P. Jain, M. T. Islam, and A. S. Alshammari, "Comparative analysis of machine learning techniques for metamaterial absorber performance in terahertz applications," *Alexandria Engineering Journal*, vol. 103, pp. 51–59, Sep. 2024, doi: 10.1016/J.AEJ.2024.05.111.

[16] S. K. Patel, J. Surve, V. Katkar, and J. Parmar, "Machine learning assisted metamaterial-based reconfigurable antenna for low-cost portable electronic devices," *Scientific Reports 2022 12:1*, vol. 12, no. 1, pp. 1–13, Jul. 2022, doi: 10.1038/s41598-022-16678-2.

[17] B. X. Khuyen *et al.*, "Multi-Layered Metamaterial Absorber: Electromagnetic and Thermal Characterization," *Photonics 2024, Vol. 11, Page 219*, vol. 11, no. 3, p. 219, Feb. 2024, doi: 10.3390/PHOTONICS11030219.

[18] Z.-X. Liu *et al.*, "Metamaterial absorber optimization method based on an artificial neural network surrogate," *Optics Express, Vol. 31, Issue 22, pp. 35594-35603*, vol. 31, no. 22, pp. 35594–35603, Oct. 2023, doi: 10.1364/OE.503010.

[19] Y. I. Abdulkarim *et al.*, "A Review on Metamaterial Absorbers: Microwave to Optical," *Front Phys*, vol. 10, p. 893791, Apr. 2022, doi: 10.3389/FPHY.2022.893791/PDF.

[20] L. Gu, H. Liu, Z. Wei, R. Wu, and J. Guo, "Optimized Design of Plasma Metamaterial Absorber Based on Machine Learning," *Photonics 2023, Vol. 10, Page 874*, vol. 10, no. 8, p. 874, Jul. 2023, doi: 10.3390/PHOTONICS10080874.

[21] Y. Yang *et al.*, "Design, characterization and fabrication of a flexible broadband metamaterial absorber based on textile," *Addit Manuf*, vol. 69, p. 103537, May 2023, doi: 10.1016/J.ADDMA.2023.103537.

[22] M. Amiri, F. Tofigh, N. Shariati, J. Lipman, and M. Abolhasan, "Wide-angle metamaterial absorber with highly insensitive absorption for TE and TM modes," *Scientific Reports 2020 10:1*, vol. 10, no. 1, pp. 1–13, Aug. 2020, doi: 10.1038/s41598-020-70519-8.

[23] S. Bhattacharyya, S. Ghosh, D. Chaurasiya, and K. V. Srivastava, "Bandwidth-enhanced dual-band dual-layer polarization-independent ultra-thin metamaterial absorber," *Appl Phys A Mater Sci Process*, vol. 118, no. 1, pp. 207–215, Jan. 2015, doi: 10.1007/S00339-014-8908-Z/FIGURES/12.

[24] S. Ghosh, T. T. Nguyen, and S. Lim, "Recent progress in angle-insensitive narrowband and broadband metamaterial absorbers," *EPJ Applied Metamaterials*, vol. 6, p. 12, 2019, doi: 10.1051/EPJAM/2019010.

[25] D. E. Wen, X. Huang, L. Guo, H. Yang, S. Han, and J. Zhang, "Quadruple-band polarization-insensitive wide-angle metamaterial absorber based on multi-layer structure," *Optik (Stuttg)*, vol. 126, no. 9–10, pp. 1018–1020, May 2015, doi: 10.1016/J.IJLEO.2015.03.005.

[26] S. Bhattacharyya, S. Ghosh, and K. V. Srivastava, "Bandwidth-Enhanced Metamaterial Absorber Using Electric Field–Driven Lc Resonator For Airborne Radar Applications," *Microw Opt Technol Lett*, vol. 55, no. 9, pp. 2131–2137, Sep. 2013, doi: 10.1002/MOP.27786.

[27] M. R. Soheilifar and R. A. Sadeghzadeh, "Design, fabrication and characterization of stacked layers planar broadband metamaterial absorber at microwave frequency," *AEU - International Journal of Electronics and Communications*, vol. 69, no. 1, pp. 126–132, Jan. 2015, doi: 10.1016/J.AEUE.2014.08.005.

[28] S. Ghosh, S. Bhattacharyya, and K. V. Srivastava, "Bandwidth-enhancement of an ultrathin polarization insensitive metamaterial absorber," *Microw Opt Technol Lett*, vol. 56, no. 2, pp. 350–355, Feb. 2014, doi: 10.1002/MOP.28122.